Length- and Defect-Dependent Fluorescence Efficiencies of Individual Single-Walled Carbon Nanotubes

Tonya K. Cherukuri, Dmitri A. Tsyboulski, and R. Bruce Weisman*

Department of Chemistry and Richard E. Smalley Institute for Nanoscale Science and Technology, Rice University, 6100 Main Street, Houston, Texas 77005, United States

ABSTRACT

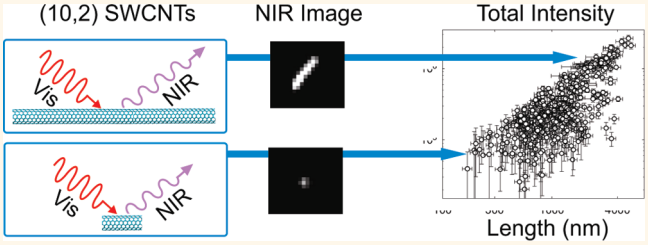

Using near-infrared fluorescence videomicroscopy with spectrally selective excitation and imaging, more than 400 individual (10,2) single-walled carbon nanotubes (SWCNTs) have been studied in unsorted liquid dispersions. For each nanotube, the spatially integrated emission intensity was measured under controlled excitation conditions while its length was found either from direct imaging or from the diffusion coefficient computed by analyzing its Brownian motion trajectory. The studied nanotubes ranged in length from 170 to 5300 nm. For any length, a wide variation in emission intensities was observed. These variations are attributed to differing densities of nanotube imperfections that cause fluorescence quenching. The brightest nanotubes at each length (presumed near-pristine) show total emission nearly proportional to length. This implies a nearly constant fluorescence quantum yield and a constant absorption cross section per carbon atom, validating conventional Beer–Lambert analysis for finding concentrations of SWCNT species. Ensemble-averaged emission is also proportional to length, but at only *ca.* 40% of the near-pristine values. Further research is needed to investigate the extrinsic effects causing wide variation in quantum yields and assess their implications for SWCNT fluorimetry.

KEYWORDS: SWCNT · carbon nanotubes · fluorescence microscopy · fluorescence efficiency · extrinsic quenching · length dependence · photoluminescence

The discovery and structural assignment in 2002 of near-infrared (near-IR) fluorescence from semiconducting single-walled carbon nanotubes (SWCNTs)[1,2] has enabled a wide range of basic and applied research projects. Unfortunately, studies of nanotube photophysics continue to be hampered by the polydispersity of bulk SWCNT samples. Because of the difficulties in controlling SWCNT growth, as-produced samples contain substantial variations in lengths, (*n*,*m*) structures (corresponding to different diameters and roll-up angles), and imperfections. It is important to understand the effects of each of these variations on nanotube spectroscopic and photophysical properties. The systematic relation between (*n*,*m*) structure and spectral transition wavelengths is well-established.[2,3] In addition, (*n*,*m*)-dependent patterns in fluorescence action cross sections have recently been uncovered and reported.[4] However, there is currently less consensus on the influence of SWCNT length on optical properties,[5,6] and the quantitative effects of imperfections on nanotube fluorescence remain poorly understood. Both of these topics are relevant not only as fundamental science but also for the practical spectrometric measurement of SWCNT concentrations in bulk samples. For example, if (as has been reported) the absorptivity or fluorescence brightness per carbon atom depends on nanotube length, then optical measurement of a sample's SWCNT content will require knowledge of its length distribution in addition to its spectra. Improved structural sorting and purification methods allow the effects of length and imperfections to be studied in bulk with fewer complications from polydispersity. However, because bulk experiments measure averages rather than full distributions of physical values, they cannot provide a complete view of the effects of interest. Here we instead report a large set of near-IR fluorescence microscopy measurements on individual, well-characterized SWCNTs that show how their fluorescence is influenced by nanotube length and imperfections. Our experimental strategy is to start with a well-dispersed but structurally unsorted sample and then use suitable choices of excitation wavelength and emission spectral filtering to restrict our observations to a single (*n*,*m*) species. A near-IR image sequence showing a freely diffusing nanotube is recorded, and the length of that nanotube is found either

* Address correspondence to weisman@rice.edu.

Received for review November 9, 2011 and accepted November 30, 2011.

Published online November 30, 2011
10.1021/nn2043516

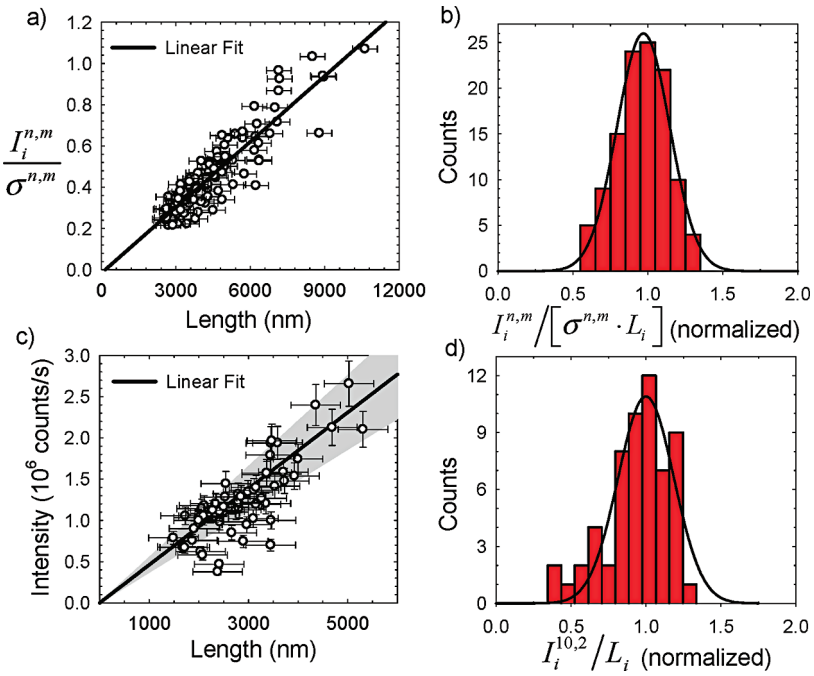

Figure 1. (a) Spatially integrated emission *vs* length for individual SWCNTs of various (*n*,*m*) types, as measured previously (ref 4). Nanotubes were selected for absence of apparent defects, and emission intensities are normalized by $\sigma^{(n,m)}$, the fluorescence action cross sections of the corresponding (*n*,*m*) structures. (b) Normalized distribution of the $I_i^{(n,m)}/\sigma^{(n,m)}$ values per unit length. The Gaussian fit has a standard deviation of 0.18. (c) Spatially integrated emission intensities of individual pristine (10,2) SWCNTs as a function of their lengths. (d) Normalized distribution of the $I_i^{(10,2)}/L_i$ values. The Gaussian fit has a standard deviation of 0.19. The shaded region in (c) represents a proportional dependence with uncertainty matching this standard deviation value.

from direct image measurements or by analyzing its trajectory to deduce its diffusion coefficient. The nanotube's total emission intensity under controlled excitation conditions is also recorded. Measurements of correlated emission intensities and lengths are then repeated and compiled for many SWCNTs until meaningful patterns emerge.

RESULTS AND DISCUSSION

In the linear regime of low to modest excitation intensities, the emission from a perfect SWCNT in a defined environment will be proportional to the incident photon irradiance. We hypothesize that the proportionality factor, which will depend on (*n*,*m*) structure, can be expressed as the number of carbon atoms in the nanotube times a length-independent fluorescence action cross section $\sigma_{FI}^{n,m}$, an intrinsic photophysical parameter that is the product of absorption cross section per carbon atom at the excitation wavelength times fluorescence quantum yield. This will be true if the quantum yield and the absorption cross section per atom are independent of nanotube length. If it is not the case, as reported by Fagan *et al.*,[5] then the familiar concept of molar absorptivity will not apply to SWCNTs, and $\sigma_{FI}^{n,m}$ values will be systematic functions of length.

Our experiments address this important point in two ways. First, we analyze a prior set of $\sigma_{FI}^{n,m}$ measurements performed on 116 "near-pristine" SWCNTs of 12 different (*n*,*m*) species and with lengths ranging from ~3 to 10 μm. These nanotubes were selected for spatial uniformity of their fluorescence emission.[3] To reveal possible variations of $\sigma_{FI}^{n,m}$ with length in this sample, we have compiled a scatter plot showing length-integrated emission intensities, $I_i^{n,m}$, *versus* length for all 116 nanotubes (Figure 1a). The length-integrated emission intensity of each nanotube has been divided by $\sigma_{FI}^{n,m}$, the average value determined for that species, to compensate for intrinsic brightness differences among (*n*,*m*) species. The data show a linear correlation between integrated emission and length, with a very small *x*-intercept of ~160 ± 220 nm. These data are analyzed further in Figure 1b, which shows a histogram of $I_i^{n,m}/[\sigma_{FI}^{n,m} \times L_i]$ values scaled to their average value. The key feature of this histogram is a normal distribution about the central value, with a relative standard deviation of 0.18. This indicates that the integrated emission data deviate only randomly, not systematically, from a linear length dependence, thereby confirming that $\sigma_{FI}^{n,m}$ values are constant over the 3−10 μm range of the data set.

Next, we made similar measurements spectrally restricted to the (10,2) SWCNTs in a polydisperse unsorted sample. We analyzed emission intensities of individual nanotubes that were long enough to measure optically using the method described earlier. We selected either near-pristine SWCNTs (those showing spatially uniform emission at our diffraction-limited resolution of ~700 nm)

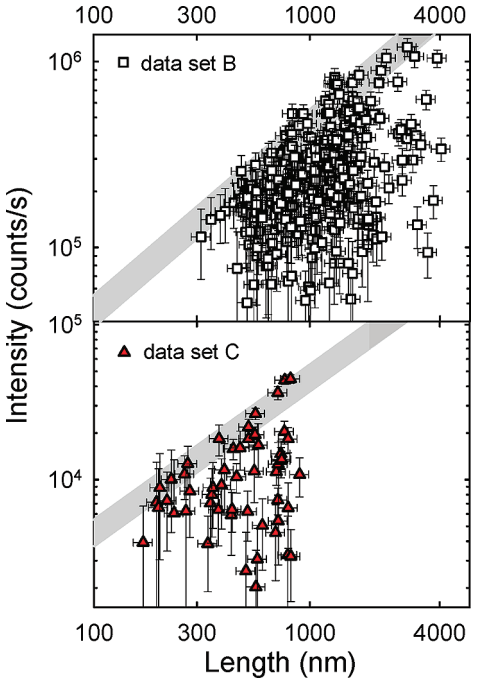

Figure 2. Intensities of individual (10,2) nanotubes as a function of their lengths. Data sets B and C, containing 298 and 52 individual nanotubes, respectively, were studied in solutions with different viscosities. The shaded region is the extrapolated linear trend shown in Figure 1c. Error bars are based on the maximum standard deviation in the D_{trans} values used to deduce length and on the experimental uncertainties in average intensity measurements.

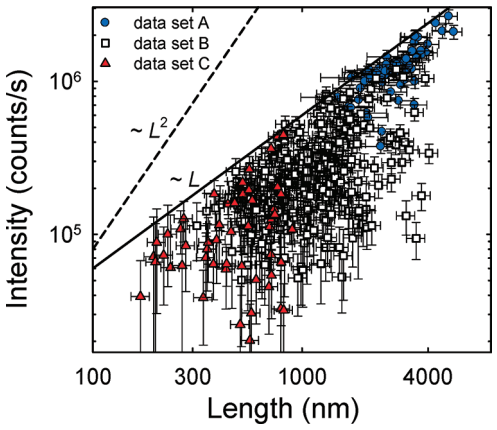

Figure 3. Log−log plot of length-dependent intensities of the 408 individual (10,2) SWCNTs in combined data sets A, B, and C. Lines representing functions proportional to L^2 and L are drawn as guides to the slope of the upper edge of the data point distribution.

or SWCNTs with relatively small regions of dimmer emission. In the latter case, we attempted to account for the local emission defects by replacing their intensities with those of adjacent regions when computing total emission. Figure 1c shows the correlated total emission intensities and lengths of 58 individual (10,2) nanotubes (data set A). A linear trend similar to that in Figure 1a can be seen. Figure 1d shows the normalized distribution histogram of $I_i^{10,2}/L_i$ values. A Gaussian fit has a standard deviation of 0.19, but the distribution is less symmetric than that of Figure 1b. Note that this data set includes SWCNTs as short as 1.5 μm, for which emission nonuniformities are difficult to detect. This accounts for some of the asymmetry in the histogram and for low-emission outliers in the plot, which are not numerous enough to substantially affect the linear fit shown in Figure 1c. The x-intercept of that fit, 100 $\pm$ 300 nm, is again zero within fitting uncertainty. The gray wedged region drawn in Figure 1c includes slopes within one standard deviation of the mean. This analysis of data from 58 near-pristine (10,2) nanotubes corroborates our finding that σ_{FI} is independent of length for longer nanotubes.

We extended this study of (10,2) SWCNTs to include lengths that were too short for direct optical measurement and were instead deduced from analysis of Brownian motions (see Methods). Figure 2 (top) shows correlated intensity and length measurements for 298 individual (10,2) nanotubes (data set B) in a solution with enhanced viscosity of 4.0 $\pm$ 0.1 mPa·s. Unlike nanotubes from data set A, these were not subject to selection criteria except for the (10,2) restriction. SWCNT lengths vary from 300 nm to 4 μm within this data set. For SWCNTs with lengths greater than 1.5 μm, we measured the intensity *versus* length correlation by two independent methods and found excellent consistency of results (see Supporting Information). From Figure 2 (top), it is clear that emission intensities vary substantially among (10,2) SWCNTs with similar lengths. We attribute these variations to quenching imperfections such as structural (growth) defects or covalent derivatization of the nanotube surface. The presence of defects or sections with different brightness within a single nanotube in data set B is evident from images of nanotubes with $L > 1.5$ μm. The quenching defect density of nanotubes is an unknown parameter that may vary significantly. Because of the high mobility of SWCNT excitons, quencher densities of 0.01 nm^{-1} are likely to significantly suppress SWCNT emission.[7−9] Thus, large variations in emission intensities of SWCNTs with similar lengths may reflect small variations in the numbers of such defects. The intrinsic length dependence of SWCNT emission is expected to be observed only for the small subset of near-pristine SWCNTs having the highest emission efficiencies. If σ_{FI} is constant over the wider range of nanotube lengths represented by this data set, then the top points in Figure 2 (top) would match the linear trend extrapolated from data set A. This trend from data set A is shown by the gray region, which does indeed encompass the brightest SWCNTs found in data set B.

Data set B includes very few nanotubes with lengths below 400 nm because of limits in our detection sensitivity. Short nanotubes not only emit less light but also move more quickly during each image exposure, spreading their emission over several image pixels and making their detection and tracking challenging. To study shorter nanotubes, we prepared a sample suspension with

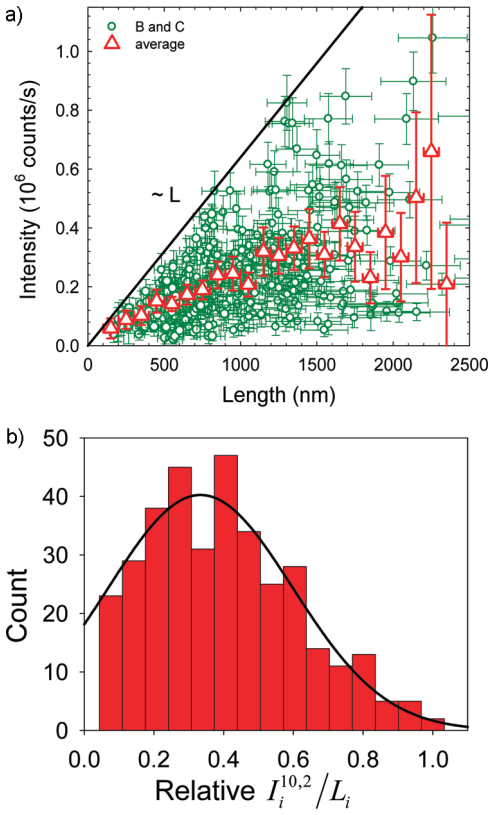

Figure 4. (a) Data for individual (10,2) SWCNTs showing integrated emission intensity *vs* length for data sets A and B (small green symbols), and emission intensities averaged over discrete 100 nm intervals (large red symbols). Relative error bars show standard errors of the means. (b) Distribution of normalized $I_i^{10,2}/L_i$ values from data sets B and C. The solid curve is a Gaussian centered at 0.33 with a fwhm of 0.53.

a higher viscosity (η = 6.3 ± 0.1 mPa·s) and measured emission intensities and lengths of an additional 52 (10,2) nanotubes (data set C). Figure 2 (bottom) shows SWCNT intensities plotted against deduced lengths ranging from 170 to 1000 nm in this sample. The results are consistent with those found from data sets A and B.

Figure 3 shows a plot combining data sets A, B, and C. Overlapping data are in excellent agreement despite differences in sample condition and measurement methods. The combined data include SWCNTs spanning a factor of 30 in length, from 170 to 5300 nm. To help gauge the dependence of integrated intensity on length, functions proportional to L and L^2 are plotted on the graph. It is clear that the uppermost data points, presumably representing near-pristine nanotubes with few fluorescence-quenching defects, follow a very nearly linear relationship between intensity and length over this range.

Typical fluorescence measurements are of course made not on individual nanotubes but on bulk samples. Data sets B and C were recorded without selection and when combined are large enough to represent the fluorescence intensity distribution of a bulk sample. To examine mean emission intensities as a function of length, we binned and averaged the measured intensities for all SWCNTs within 100 nm length intervals. In the length range from 300 to 1700 nm, each such bin contains 10 to 35 nanotubes. Figure 4a shows a plot of the resulting average values (as red triangles) *versus* length, along with all of the individual nanotube data. The averaged SWCNT intensity values show an approximately linear dependence on length. The trend through the average values has a negative intercept on the length axis. We believe that the negative intercept results from the sensitivity limits of our imaging, which make short SWCNTs with defects harder to detect. This causes the brightest short nanotubes to be overrepresented and moves the intercept to lower values. Regardless, experimental data for both pristine nanotubes and averaged ensemble intensities reveal a linear trend of integrated emission with length.

Figure 4a also gives insight on another important topic: the variations in fluorescence brightness among SWCNTs having the same (*n*,*m*) structure and length. We examined this fluorescence efficiency distribution by compiling a histogram showing the frequency of $I_i^{10,2}/L_i$ values (normalized to the maximum, near-pristine value) for combined data sets B and C. As seen in Figure 4b, this distribution is quite wide, with a small number of nanotubes showing maximal brightness (bar at 1.0), a much larger number showing less than 10% of the maximal brightness (bar at 0.07), and most falling between these limits. The mean relative brightness in the data set is approximately 40% of maximum. The distribution indicates that most SWCNTs grown and processed by the methods used here are substantially affected by quenching centers, and that only a small fraction of nanotubes show fluorescence undiminished by extrinsic quenching. Note that the data in Figure 4b do not reflect reduced fluorescence quantum yields from energy transfer within bundles because the data acquisition methods select strongly for individualized SWCNTs.

It is necessary to consider error sources that could influence our findings on length-dependent SWCNT emission. One source of systematic bias is the tendency to overlook nanotubes that give the dimmest images. These would include the shortest nanotubes and those with high densities of quenching defects. Such omissions would not affect the uppermost data in Figure 4a but might cause the lowest intensity bars in the histogram of Figure 4b to be underestimated. When deducing nanotube lengths from diffusional data, the uncertainty in hydrodynamic diameter used in eq 1 can cause no more than 10% error in length over the entire range of data sets B and C. A more serious source of error might be a length variation of the wall-drag viscosity correction factor. Although we have assumed that the same apparent viscosity applies to SWCNTs over a wide length range, this has been demonstrated experimentally only for rigid rods longer than 1 μm in this and earlier studies.[10−12] If wall-drag effects are

actually reduced or absent for the shortest nanotubes in our samples, we would have underestimated their lengths, possibly by as much as ~35%. However, other investigators have found significant wall-drag effects for particles much smaller than the gap dimension.[12,13] This suggests that errors in our deduced lengths of short nanotubes are too minor to alter the main finding that σ_{FI} values are essentially constant.

We interpret this result as implying a constant absorption cross section per carbon atom and an intrinsic fluorescence quantum yield that is nearly constant over the range of lengths studied here. Two earlier studies of bulk SWCNT dispersions reached conclusions different from this. Using samples that were heavily sonicated and then fractionated by gel electrophoresis, Heller *et al.* reported in 2004 that SWCNT fluorescence quantum yield increases exponentially (by a factor greater than 10) as average length increases from 92 to 440 nm.[6] This finding is highly inconsistent with the constant quantum yields implied by our Figure 4a data for both near-pristine and ensemble-averaged SWCNTs. Several factors may contribute to this discrepancy. The samples used by Heller *et al.* were sonicated for 10 h, as compared to 3 min for ours. Sidewall damage from this extensive agitation likely introduced additional quenching sites, possibly with higher densities in the shortest SWCNTs. It is also possible that the electrophoretic separation process sorted the sample fractions not only by length but also by another property (such as surface derivatization) correlated with fluorescence quenching. By contrast, the samples used in our study were never physically fractionated. In 2007, Fagan *et al.* reported an optical study of fractionated bulk SWCNT samples with average lengths from 20 to 600 nm. They concluded that the per carbon atom absorption, fluorescence, and Raman signals all increase approximately linearly with nanotube length in this range, in contrast to our finding of constant σ_{FI}. Because the samples used in that study contained SWCNT masses too low for direct gravimetric determination, their concentrations were instead deduced from absorbance readings near 1700 nm, under the assumption that such signals are proportional to carbon content and independent of SWCNT structure. We suggest that a failure of that assumption caused errors in the deduced SWCNT concentrations and the discrepancy with our findings. It is now known that absorbance backgrounds in SWCNT dispersions have multiple sources and need not be proportional to total carbon concentration.[14] We also note an internal inconsistency in the results reported by Fagan *et al.*: if a fundamental photophysical effect actually makes absorption cross sections per atom increase linearly with nanotube length, then it should also increase fluorescence quantum yields, which involve a similar cross section for the emission transition. This would give a quadratic length dependence of fluorescence intensity instead of the reported linear result.[5] Our experiments avoid the challenges and pitfalls of estimating bulk sample concentrations because they are direct measurements on "samples" consisting of individual SWCNTs of known (*n*,*m*) identity and observed lengths.

If the ends of nanotubes act as sites for exciton recombination, then exciton mobility will cause reduced fluorescence quantum yields for nanotubes short enough to allow many excitons to reach an end during their lifetime. As exciton excursion ranges in near-pristine SWCNTs have been experimentally found in the range of 100 to 200 nm,[8,9,15] significantly reduced quantum yields should be apparent for SWCNTs with lengths on this scale, as reported by Hertel *et al.*[16] In contrast to the surprising exponential increase of quantum yield with length reported by Heller *et al.*, the Hertel quantum yield results for (6,5) SWCNTs show an expected asymptotic approach to a constant value as nanotube length increases. Our results qualitatively agree with that finding, but sparse data for short nanotubes prevent us from quantitatively tracing quantum yield *versus* length at small length values. We note that measurements on bulk samples are averaged along the length axis by the length polydispersity present in each experimental fraction. In addition, the corresponding bulk intensity or quantum yield values also represent ensemble averages over the distribution of sidewall quencher density, which may itself depend on length and processing. It may therefore prove valuable to investigate the short length variation of quantum yields by further single-nanotube studies.

Our results have several implications for the quantitative characterization of bulk SWCNT samples through absorption and fluorescence spectroscopy. First, we presume that other semiconducting SWCNT species will show the same qualitative photophysical properties found here for (10,2) nanotubes. This means that pristine SWCNTs of the lengths that predominate in typical samples will have constant absorption coefficients per carbon atom and nearly constant fluorescence quantum yields, although both of these quantities will depend on (*n*,*m*) identity. One can therefore apply conventional relations, such as the Beer–Lambert Law, to deduce total carbon concentrations of specific (*n*,*m*) species from absorption data once absorptivity values are known. For fluorescence, our study reveals a wide and previously unsuspected variation in quantum yields among SWCNTs having the same (*n*,*m*) identity and length. This emissive heterogeneity is found for all lengths and is attributed to variations in the densities of local quenching defects produced in the nanotubes during growth and/or subsequent processing. The average quantum yield in our samples was approximately 40% of the maximum observed for the brightest nanotubes. This ratio of average to maximum quantum yield will likely vary with nanotube source and processing history. However, if that ratio remains nearly the same among (*n*,*m*) species within a single sample, then fluorimetric analysis can provide quantitative (*n*,*m*) concentration distributions based on measured bulk emission strengths from the various species corrected by relative $\sigma_{FI}^{n,m}$ values found from

studies on individual near-pristine SWCNTs.[4] Analysis may be more complex if samples contain length distributions with short average values that vary with diameter.

Our study suggests the need for further investigations to compare the defect-induced quantum yield distributions arising from different nanotube growth methods and processing protocols. Choice of surfactant coating is also known to affect SWCNT intrinsic quantum yields,[17,18] and it seems possible that coatings that give lower average SWCNT fluorescence will reduce the sensitivity to extrinsic quenching defects. This may cause sharper distributions of quantum yields and milder end-quenching effects.

CONCLUSIONS

We have measured fluorescence emission intensities and lengths of more than 400 individual (10,2) SWCNTs spanning a factor of 30 in length. The results show that the brightest nanotubes of all lengths have nearly the same value of fluorescence action cross section, which suggests a constant absorption cross-section per carbon atom and a nearly constant fluorescence quantum yield. The normal relations used for quantitative spectrometric analysis therefore can be applied to SWCNT samples. In addition, we find a very wide distribution of fluorescence intensities at all nanotube lengths and an ensemble-averaged emission that is only ~40% that of the brightest nanotubes. These wide variations in (10,2) fluorescence quantum yields are suggested to reflect a broad distribution in the density of quenching defect sites. The unique ability of single-nanotube measurements to reveal such distributions will lead to improved understanding of intrinsic and extrinsic effects in SWCNT photophysics.

METHODS

Suspensions of individualized SWCNTs were prepared by agitating ~1 mg of raw HiPco SWCNTs (Rice reactor batch HPR 162.8) in 10 mL of 1% aqueous SDBS with a tip sonicator (Microson XL 2000) for 3 min at 8 W. To prepare samples enriched in long individualized SWCNTs, the sonication time was limited to 5 s. After sonication, samples were mildly centrifuged for 3 min at 8000 rpm (Biofuge 13, Heraeus Sepatech) to remove large SWCNT bundles from the supernatant. The resulting stock suspension (peak optical density ~0.5) was diluted by a factor of ~25 for measurements. A 100 μL portion of the diluted SWCNT suspension was added to 5.0 mL of a 20% glucose/13% sucrose/1% SDBS solution to increase the viscosity to 4.0 ± 0.1 mPa·s. A second sample of higher viscosity (η_s = 6.3 ± 0.1 mPa·s) was prepared similarly using a 25% glucose/16% sucrose/1% SDBS solution. Suspension viscosities were calculated from a Cannon-Fenske routine viscometer (size 150) and density measurements that were made at 295 K, the temperature used for all experiments. The presence of glucose and sucrose did not change the SWCNT emission intensity. Thin liquid films were prepared for microscopic imaging by spreading 1.3 μL of the sample suspension between a glass slide and a coverslip, giving a gap height between surfaces of 2.9 μm, as measured by focus position differences between the two interfaces. Edges were sealed with vacuum grease to prevent liquid evaporation and convection, and the samples were mounted on a modified inverted Nikon TE-2000U microscope for study. Further details can be found in Supporting Information.

We selected (10,2) nanotubes for this study because they are adequately abundant in our samples and were previously found to have high fluorimetric brightness.[4] Using a customized fluorescence microscope/spectrometer system described earlier,[19] we excited the sample with a linearly polarized diode laser whose 730 nm emission wavelength was close to the 737 nm peak of the (10,2) E_{22} transition. The excitation intensity at the sample was ~100 W/cm^2. Emission from the sample was collected with a Nikon 60×/1.0 NA water-immersion objective lens and passed through a dichroic beamsplitter and a 946 nm long-pass filter. The light was then directed to a small spectrograph (J-Y C140) coupled to an InGaAs linear array detector (Roper Scientific OMA-V) to capture local near-IR spectra. Alternatively, the light could be directed through a band-pass filter (10 nm wide centered at 1050 nm) to isolate the 1053 nm E_{11} fluorescence from (10,2) SWCNTs before wide-field imaging with a liquid nitrogen cooled InGaAs camera (Roper Scientific OMA-V 2D). Using this near-IR sensitive camera, we recorded 2000 sequential images of a 25 × 25 μm area showing a SWCNT diffusing in liquid suspension. SWCNTs longer than ~1.5 μm were also imaged with additional 1.5× magnification (90× total) to improve the precision of optical length measurements. The spatially integrated intensity of each nanotube was measured from 60× fluorescence image sequences.

We deduced the lengths of nanotubes shorter than 1.5 μm from translational diffusion coefficients using custom Matlab routines to analyze image sequences of the nanotubes undergoing free Brownian motion.[11,19] Because (10,2) SWCNTs have a persistence length exceeding 30 μm,[20] all of the nanotubes used in our study can accurately be treated as rigid rods, for which translational diffusion coefficients obey the following relation:[11,21,22]

$$D_{TR} = \frac{k_B T}{6\pi\eta_s} \times \frac{2\ln(L/d) - \gamma_{||} - \gamma_{\perp}}{L} \quad (1)$$

Here, k_B is the Boltzmann constant, T is the sample temperature, η_s is the suspension viscosity, L is the nanotube length, d is the hydrodynamic diameter of the surfactant-coated nanotube (taken to be 5 ± 2 nm),[1,11,23] and $\gamma_{||}$ and $\gamma_{\perp}$ are hydrodynamic end correction coefficients.[22] The sample temperature and viscosity are measured independently. Thus, nanotube lengths can be found by measuring D_{TR} of individual nanotubes under known experimental conditions. Note that because of the logarithmic dependence on L/d in eq 1, the uncertainty in nanotube diameter causes an uncertainty in D_{TR} of only ~12% for 200 nm long SWCNTs and less for longer nanotubes. Figure 5a shows four examples of mean squared displacement (MSD) graphs for individual nanotubes, each computed from a 2000 frame trajectory. The slope of the linear portion of the MSD plot equals $4D_{TR}$ because observed trajectories are two-dimensional projections of three-dimensional Brownian motion. Our deduced D_{TR} values typically have estimated relative uncertainties of 2−10%.

When computing L from D_{TR}, it is important to consider the wall-drag effect that impedes translational diffusion of particles in a confined geometry.[10,11] This is usually accounted for by using a higher effective solution viscosity, termed apparent viscosity, in eq 1. To determine the apparent viscosity in our system, we recorded diffusional trajectories of a number of long nanotubes (between 1.5 and 5 μm) whose lengths were measured optically, then determined their D_{TR} values from trajectory analysis, and found η_s values that satisfied eq 1. This gave apparent viscosities for the two solutions used in our experiments of 5.3 ± 1.0 and 9.2 ± 1.1 mPa·s, which are higher than their measured bulk viscosities by factors of 1.3 ± 0.3 and 1.5 ± 0.2 (see Supporting Information). We used these apparent

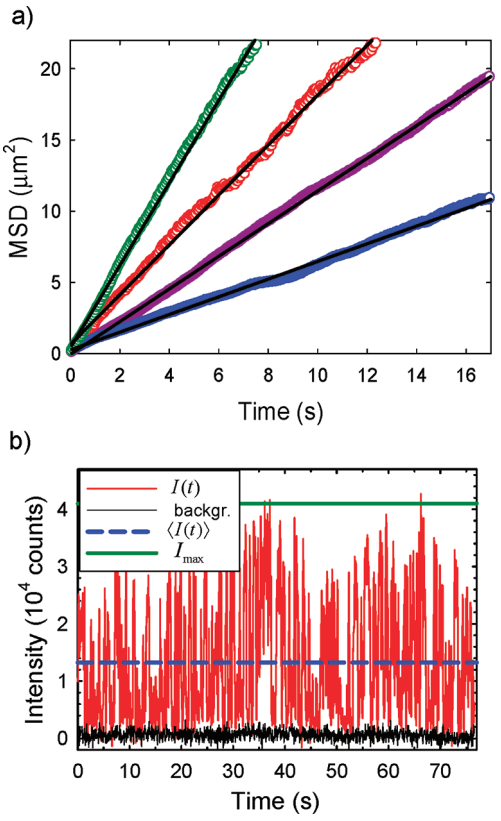

Figure 5. (a) Mean-squared displacement (MSD) traces for several representative (10,2) nanotubes. The slopes equal $4D_{TR}$. (b) Time-resolved emission signal $I(t)$ from a nanotube approximately 1 μm in length. The average emission $\langle I(t)\rangle$ (dashed blue line) is used to calculate maximum emission intensity of the nanotube, I_{max} (solid green line), as explained in the text.

viscosity values with eq 1 to deduce the lengths of other nanotubes from diffusional measurements.

Our trajectory tracking and fluorescence intensity measurements benefit from the fact that SWCNTs in appropriate environments are highly photostable emitters that exhibit no intermittency for excitation intensities below ~1 kW/cm^2.[8,24] SWCNTs have high optical anisotropies because the dominant optical transitions are parallel to the nanotube axis;[25−27] the experimentally measured optical anisotropy is 0.95 for (10,2) nanotubes excited at 730 nm.[28] When excited with linearly polarized light, SWCNTs in liquid suspension will show fluorescence blinking as they randomly reorient relative to the polarization direction. The faster rotational motions of short nanotubes lead to more rapid averaging over the range of orientations, which reduces observed emission modulation at a given time resolution. Regardless of rotation speed, the time-averaged SWCNT emission intensity is $\langle I(t)\rangle = \alpha \times \beta(L) \times I_{max}$, where I_{max} is the maximized intensity when the nanotube is aligned in the polarization plane of the excitation beam and perpendicular to the observation axis, $\alpha = 0.315$ is a proportionality constant that depends only on the experimental geometry and anisotropic optical properties of the emitter, and $\beta(L)$ is a length-dependent correction coefficient that accounts for restricted SWCNT rotation in confined geometries.[11] In a thin liquid layer of thickness H, the rotational motion becomes restricted predominantly to a plane as nanotube length increases. As a result, the $\langle I(t)\rangle/I_{max}$ ratio changes in a predictable fashion from 0.315 (because $\beta(L) = 1$ for $L \ll H$) to ~0.53 (for $L \gg H$). For SWCNTs with lengths below 1 μm and H = 2.9 μm, the $\beta(L)$ correction parameter is relatively small, less than 1.1. Hence, the I_{max} value of each mobile nanotube may be reliably deduced from measurements of $\langle I(t)\rangle$ and L. Figure 5b shows an example of a time-resolved fluctuating emission signal from an individual (10,2) nanotube with an estimated length of 1.0 ± 0.1 μm. The dashed blue line shows the average emission signal, $\langle I(t)\rangle$, used to calculate maximum I_{max} (solid green line). In this case, the reorientation modulation is well-resolved and signals vary from 0 to I_{max}.

Acknowledgment. This work was supported by the Welch Foundation (Grant C-0807), the National Science Foundation (Grants CHE-0809020 and CHE-1112374), and Applied Nano-Fluorescence, LLC. We thank J. Streit for helpful discussions.

Supporting Information Available: Details of methods used for determining nanotube lengths and emission intensities. This material is available free of charge *via* the Internet at http://pubs.acs.org.

REFERENCES AND NOTES

1. O'Connell, M. J.; Bachilo, S. M.; Huffman, C. B.; Moore, V.; Strano, M. S.; Haroz, E.; Rialon, K.; Boul, P. J.; Noon, W. H.; Kittrell, C.; *et al.* Band-Gap Fluorescence from Individual Single-Walled Carbon Nanotubes. *Science* **2002**, *297*, 593–596.
2. Bachilo, S. M.; Strano, M. S.; Kittrell, C.; Hauge, R. H.; Smalley, R. E.; Weisman, R. B. Structure-Assigned Optical Spectra of Single-Walled Carbon Nanotubes. *Science* **2002**, *298*, 2361–2366.
3. Weisman, R. B.; Bachilo, S. M. Dependence of Optical Transition Energies on Structure for Single-Walled Carbon Nanotubes in Aqueous Suspension: An Empirical Kataura Plot. *Nano Lett.* **2003**, *3*, 1235–1238.
4. Tsyboulski, D.; Rocha, J.-D. R.; Bachilo, S. M.; Cognet, L.; Weisman, R. B. Structure-Dependent Fluorescence Efficiencies of Individual Single-Walled Carbon Nanotubes. *Nano Lett.* **2007**, *7*, 3080–3085.
5. Fagan, J. A.; Simpson, J. R.; Bauer, B. J.; DePaoliLacerda, S. H.; Becker, M. L.; Chun, J.; Migler, K. B.; Hight Walker, A. R.; Hobbie, E. K. Length-Dependent Optical Effects in Single-Wall Carbon Nanotubes. *J. Am. Chem. Soc.* **2007**, *129*, 10607–10612.
6. Heller, D. A.; Mayrhofer, R. M.; Baik, S.; Grinkova, Y. V.; Usrey, M. L.; Strano, M. S. Concomitant Length and Diameter Separation of Single-Walled Carbon Nanotubes. *J. Am. Chem. Soc.* **2004**, *126*, 14567–14573.
7. Dukovic, G.; White, B. E.; Zhou, Z. Y.; Wang, F.; Jockusch, S.; Steigerwald, M. L.; Heinz, T. F.; Friesner, R. A.; Turro, N. J.; Brus, L. E. Reversible Surface Oxidation and Efficient Luminescence Quenching in Semiconductor Single-Wall Carbon Nanotubes. *J. Am. Chem. Soc.* **2004**, *126*, 15269–15276.
8. Cognet, L.; Tsyboulski, D.; Rocha, J.-D. R.; Doyle, C. D.; Tour, J. M.; Weisman, R. B. Stepwise Quenching of Exciton Fluorescence in Carbon Nanotubes by Single-Molecule Reactions. *Science* **2007**, *316*, 1465–1468.
9. Siitonen, A. J.; Tsyboulski, D. A.; Bachilo, S. M.; Weisman, R. B. Surfactant-Dependent Exciton Mobility in Single-Walled Carbon Nanotubes Studied by Single-Molecule Reactions. *Nano Lett.* **2010**, *10*, 1595–1599.
10. Li, G.; Tang, J. X. Diffusion of Actin Filaments within a Thin Layer between Two Walls. *Phys. Rev. E* **2004**, *69*, Article no. 061921.
11. Tsyboulski, D. A.; Bachilo, S. M.; Kolomeisky, A. B.; Weisman, R. B. Translational and Rotational Dynamics of Individual Single-Walled Carbon Nanotubes in Aqueous Suspension. *ACS Nano* **2008**, *2*, 1770–1776.
12. Marshall, B. D.; Davis, V. A.; Lee, D. C.; Korgel, B. A. Rotational and Translational Diffusivities of Germanium Nanowires. *Rheol. Acta* **2009**, *48*, 589–596.
13. Lin, B.; Yu, J.; Rice, S. A. Direct Measurements of Constrained Brownian Motion of an Isolated Sphere between Two Walls. *Phys. Rev. E* **2000**, *62*, 3909–3919.
14. Naumov, A. V.; Ghosh, S.; Tsyboulski, D. A.; Bachilo, S. M.; Weisman, R. B. Analyzing Absorption Backgrounds in Single-Walled Carbon Nanotube Spectra. *ACS Nano* **2011**, *5*, 1639–1648.

15. Siitonen, A. J.; Tsyboulski, D. A.; Bachilo, S. M.; Weisman, R. B. Dependence of Exciton Mobility on Structure in Single-Walled Carbon Nanotubes. *J. Phys. Chem. Lett.* **2010**, *1*, 2189–2192.
16. Hertel, T.; Himmelein, S.; Ackermann, T.; Stich, D.; Crochet, J. Diffusion Limited Photoluminescence Quantum Yields in 1-D Semiconductors: Single-Wall Carbon Nanotubes. *ACS Nano* **2010**, *4*, 7161–7168.
17. Moore, V. C.; Strano, M. S.; Haroz, E. H.; Hauge, R. H.; Smalley, R. E. Individually Suspended Single-Walled Carbon Nanotubes in Various Surfactants. *Nano Lett.* **2003**, *3*, 1379–1382.
18. Tsyboulski, D. A.; Bakota, E. L.; Witus, L. S.; Rocha, J. D. R.; Hartgerink, J. D.; Weisman, R. B. Self-Assembling Peptide Coatings Designed for Highly Luminescent Suspension of Single-Walled Carbon Nanotubes. *J. Am. Chem. Soc.* **2008**, *130*, 17134–17140.
19. Tsyboulski, D. A.; Bachilo, S. M.; Weisman, R. B. Versatile Visualization of Individual Single-Walled Carbon Nanotubes with Near-Infrared Fluorescence Microscopy. *Nano Lett.* **2005**, *5*, 975–979.
20. Fakhri, N.; Tsyboulski, D. A.; Cognet, L.; Weisman, R. B.; Pasquali, M. Diameter-Dependent Bending Dynamics of Single-Walled Carbon Nanotubes in Liquids. *Proc. Natl. Acad. Sci. U.S.A.* **2009**, *106*, 14219–14223.
21. Broersma, S. Viscous Force Constant for a Closed Cylinder. *J. Chem. Phys.* **1960**, *32*, 1632–1635.
22. Broersma, S. Viscous Force and Torque Constants for a Cylinder. *J. Chem. Phys.* **1981**, *74*, 6989–6990.
23. Richard, C.; Balavoine, F.; Schultz, P.; Ebbesen, T. W.; Mioskowski, C. Supramolecular Self-Assembly of Lipid Derivatives on Carbon Nanotubes. *Science* **2003**, *300*, 775–778.
24. Hartschuh, A.; Pedrosa, H. N.; Novotny, L.; Krauss, T. D. Simultaneous Fluorescence and Raman Scattering from Single Carbon Nanotubes. *Science* **2003**, *301*, 1354–1356.
25. Miyauchi, Y.; Oba, M.; Maruyama, S. Cross-Polarized Optical Absorption of Single-Walled Nanotubes by Polarized Photoluminescence Excitation Spectroscopy. *Phys. Rev. B* **2006**, *74*, 205440.
26. Lefebvre, J.; Fraser, J. M.; Finnie, P.; Homma, Y. Photoluminescence from an Individual Single-Walled Carbon Nanotube. *Phys. Rev. B* **2004**, *69*, Article no. 075403.
27. Casey, J. P.; Bachilo, S. M.; Moran, C. H.; Weisman, R. B. Chirality-Resolved Length Analysis of Single-Walled Carbon Nanotube Samples through Shear-Aligned Photoluminescence Anisotropy. *ACS Nano* **2008**, *2*, 1738–1746.
28. Leeuw, T. K. Ph.D. Dissertation, Rice University, 2008.